Experimental IR spectrum

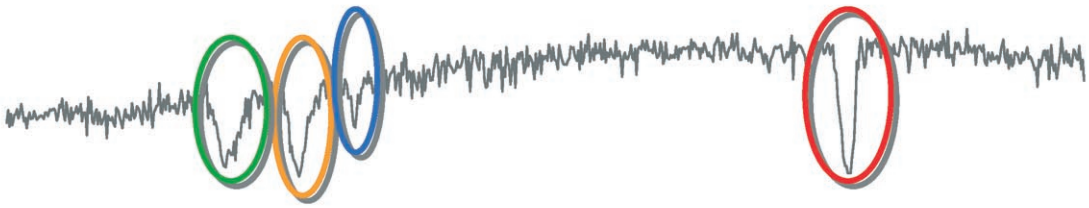

Phe-Gly-Gly

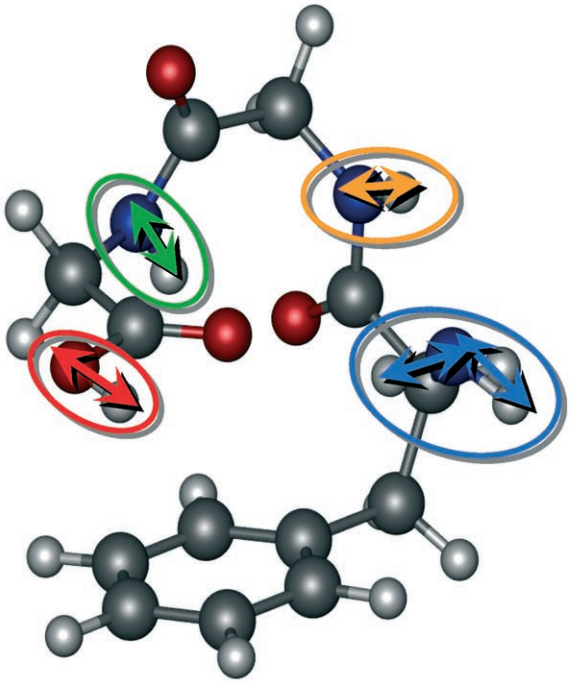

ab initio calculations

For more information see the following pages

CHEMISTRY
A EUROPEAN JOURNAL

DOI: 10.1002/chem.200500465

VIP

Structure and IR Spectrum of Phenylalanyl–Glycyl–Glycine Tripetide in the Gas-Phase: IR/UV Experiments, Ab Initio Quantum Chemical Calculations, and Molecular Dynamic Simulations

D. Řeha,[a] H. Valdés,[a] J. Vondrášek,[a] P. Hobza,*[a] Ali Abu-Riziq,[b] Bridgit Crews,[b] and Mattanjah S. de Vries[b]

Abstract: We investigated the potential-energy surface (PES) of the phenylalanyl–glycyl–glycine tripeptide in the gas phase by means of IR/UV double-resonance spectroscopy, and quantum chemical and statistical thermodynamic calculations. Experimentally, we observed four conformational structures and we recorded their IR spectra in the spectral region of 3000–4000 cm^{-1}. Computationally, we investigated the PES by a combination of molecular dynamics/quenching procedures with high-level correlated ab initio calculations. We found that neither empirical potentials nor various DFT functionals provide satisfactory results. On the other hand, the approximative DFT method covering the dispersion energy yields a reliable set of the most stable structures, which we subsequently investigated with an accurate, correlated ab initio treatment. The global minimum contains three moderately strong intramolecular hydrogen bonds and is mainly stabilized by London dispersion forces between the phenyl ring, the carboxylic acid group, and various peptide bonds. A proper description of the last type of interaction requires accurate correlated ab initio calculations, including the complete basis set limit of the MP2 method and CCSD(T) correction terms. Since in our beam experiments the conformations are frozen by cooling from a higher temperature, it is necessary to localize the most stable structures on the free-energy surface rather than on the PES. We used two different procedures (rigid rotor/harmonic oscillator/ideal gas approximation based on ab initio characteristics and evaluation of relative populations from the molecular dynamic simulations using the AMBER potential) and both yield four structures, the global minimum and three local minima. These four structures were among the 15 most energetically stable structures obtained from accurate ab initio optimization. The calculated IR spectra for these four structures agree well with the experimental frequencies, which validates the localization procedure.

Keywords: ab initio calculations · amino acids · gas-phase chemistry · IR spectroscopy · peptides

Introduction

The formation of protein secondary and tertiary structure depends on chemical and physical constraints imposed by the individual properties of the protein building blocks; that is, the 20 DNA-coded amino acids and their sequence in the polypeptide chain. In spite of considerable effort to elucidate the nature of the forces that determine the conformer states of amino acids in a particular context of a protein or short peptide, the issue remains unresolved.

Prediction of side-chain conformations plays an essential role in the modeling of protein structure. A number of prevailing approaches utilize rotamer libraries. The basic idea of this concept, which simplifies the prediction problem, is the grouping of side-chain positions in a relatively small number of statistically likely orientations called rotamers. These rotamers generally correspond to the minimum-energy positions expected for tetrahedral or trigonal carbon atoms.[1]

Tripeptides can represent efficient building blocks for protein-structure prediction. A tripeptide constitutes a minimal

[a] D. Řeha, Dr. H. Valdés, Dr. J. Vondrášek, Prof. P. Hobza
Institute of Organic Chemistry and Biochemistry
Academy of Sciences of the Czech Republic and
Center for Biomolecules and Complex Molecular Systems
166 10 Prague 6 (Czech Republic)
Fax: (+420) 220-410-320
E-mail: pavel.hobza@uochb.cas.cz

[b] A. Abu-Riziq, B. Crews, Prof. M. S. de Vries
Department of Chemistry and Biochemistry
University of California Santa Barbara, CA 93106 (USA)

Supporting information for this article is available on the WWW under http://www.chemeurj.org/ or from the author.

model containing all important forces resulting in distinct conformer states of the participating amino acids. A particular tripeptide contains all necessary factors that influence the behavior of the rotamer, maintain the interaction of side-chain with the main chain, and take into account φ and ψ preferences of allowed regions in protein structures. Recent findings show that there is relative structural rigidity between Cα and Cβ atoms in some tripeptides.[2] The carrier of such structural rigidity is often a hydrophobic residue; however, there are also tripeptides with polar chains that form rigid structures.

Tripeptides containing at least one aromatic ring are of special interest, because of a possible strong interaction between delocalized π electrons of the aromatic ring with peptide bonds. It has been recently shown[3,4] that attraction between phenylalanine and a peptide bond modeled by *N*-methyl formamide is surprisingly large, ranging up to about 10 kcal mol^{-1}. A proper description of this attraction originating in London dispersion forces requires the performance of high-level correlated ab initio methods. Popular DFT methods are of limited use, since these methods do not cover the dispersion attraction.[4]

Experimentally, a lot of work has been reported on amino acids and model peptides.[5–11] For those systems, the conformational landscapes can be explored with quite satisfactory agreement between theory and experiment in most cases.[12] The smallest tripeptide we can study by spectroscopic methods in the gas phase is phenylalanyl–glycyl–glycine (FGG). The system needs to contain a chromophore, and phenylalanine is the smallest aromatic amino acid; for the other residues we add glycine residues, the smallest amino acids. Thus this combination provides us with the smallest tripeptide for which the computational treatment can be performed at the highest theoretical level allowing comparison with experiment. At the same time, FGG is already a very complex molecule, because of its very extensive conformational landscape. In fact, this molecule can serve as a testing ground for computations of a system of this magnitude.

In addition to their biological importance as building blocks of peptides and proteins, these types of molecules are also of interest from a purely chemical point of view, because they form typical multiconformer systems with numerous local minimum structures associated with different conformational arrangements of the backbone and the side-chain.

In the present paper we report the experimental as well as theoretical investigation of the phenylalanyl–glycyl–glycine tripeptide.

Experimental Section

The experimental setup has been described elsewhere.[13] We obtained FGG from Sigma–Aldrich and used it without further purification. In brief, we prepared samples by applying the neat compound to the surface of a graphite substrate. To bring the molecules into the gas phase, we employed laser desorption by using a Nd:YAG laser operating at its fundamental wavelength (1064 nm). The laser was attenuated to 1 mJ cm^{-2} and focused to a spot approximately 0.5 mm diameter 2 mm in front of a pulsed nozzle. We translated the sample in order to expose fresh sample to successive laser shots. The nozzle consisted of a pulsed valve with a nozzle diameter of 1 mm and a backing pressure of about 5 atm of argon drive gas.

To obtain a resonant two-photon ionization (R2PI) spectrum, we used a frequency-doubled dye laser and detected the photoions in a time-of-flight mass spectrometer. By monitoring specific mass peaks while varying the two-photon ionization wavelength, we obtained mass-selected excitation spectra. We performed double-resonance spectroscopy by applying two successive laser pulses separated by a delay of about 200 ns.[14,15] As a result of this delay, we obtained two peaks in the time-of-flight spectrum that could be monitored individually. The first laser pulse served as an intense "burn" laser, and was scanned over the desired wavelength region, while the delayed laser was used as the "probe" laser and was fixed on one resonance. The burn laser depleted the ground state, and when both lasers were tuned to a resonance of the same conformer, this caused a decrease in the signal of the probe laser. To obtain IR spectra for each conformer, we used IR/UV double-resonance spectroscopy by employing an IR laser as the burn laser. For this purpose we used an OPO system (LaserVision) pumped by a Nd:YAG laser. The output of the OPO system was 8 mJ per pulse and the bandwidth was 3 cm^{-1}.

Computational Methods

Empirical potentials: We used the Cornell et al. potential in the original parameterization.[16] We determined the atomic charges of the FGG tripeptide using the procedure recommended by the authors of the AMBER force field; that is, the restrained electrostatic potential fitting procedure (RESP)[17] at the HF/6–31G* level. The charges of FGG are listed in Table S1 in the Supporting Information.

We used the CHARMM program as a part of Accelrys software package[18] and environment with two CHARMM force fields parameters.[19] The force field engine used a classical empirical energy function as well as a polarizable version of the function. All atomic parameters including partial charges were taken as default CHARMM parameters.

SCC-DFTB-D: Our approach was based on a combination of the approximate self-consistent charge, density functional tight-binding (SCC-DFTB-D) method[20] with empirical dispersion energy. The inclusion of an empirical dispersion term improved the major traditional deficiency of DFT methods, namely the omission of dispersion energy. Another advantage of the SCC-DFTB-D method is its computational efficiency, which allows its use in MD simulations for small systems (up to 400 atoms). A more detailed description of this method can be found in reference [21].

Molecular dynamics/quenching (MD/Q) calculations: For the present system we performed two types of molecular dynamics/quenching (MD/Q) calculations. The first calculation combines MD/Q with the Cornell et al. force field,[16] under the condition of constant total energy; that is, in a microcanonical NVE ensemble (N, V, and E refer to the number of particles, volume, and energy, respectively). We chose the total energies to correspond to an average temperature of 1000 K. We also employed the MD/Q method by using the SCC-DFTB-D approach.[20,21] The SCC-DFTB-D MD run was performed with scaled velocities according to a temperature of 900 K. The basic procedure of quenching consists of stopping the MD simulation repeatedly after a limited number of steps, removing the kinetic energy term, and then performing a nonrestricted minimization by using the conjugate gradient method. The energies and coordinates of the resulting minima are stored and subsequently the MD simulation continues from the point at which it was stopped. A more detailed description of the procedure can be found in reference [22].

The MD/Q procedure can serve to describe not only the PES but also the free-energy surface (FES). In the latter case one determines the population of individual energy minima during a long MD/Q simulation. This population is directly proportional to the free energy of the system. Long runs of the MD/Q simulations allow construction of the free-energy

surface. The ultimate quality of the free-energy surface depends on the quality of the empirical potential used.

The PES of the FGG tripeptide is very complex and it may happen that several energetically quite similar structures have very different geometries. Therefore, an accurate sorting and selection procedure had to be developed. After performing the MD/Q run, we sorted all structures not only on the basis of energy, but also on the basis of geometry. This procedure reduced the initial set of energy minimized structures to a set of geometrically distinct structures.

Correlated ab initio quantum chemical calculations: We carried out geometry optimizations using the approximate resolution of the identity MP2 (RI-MP2) method[23–25] together with cc-pVXZ (X = D, T) Dunning's basis sets.[26,27] We have shown[28] that absolute as well as relative RI-MP2 energies of DNA bases and base pairs differ only marginally from the exact MP2 ones, while the time saving is as large as one order of magnitude. The use of systematically improved AO basis sets allows the extrapolation of total energies to the complete AO basis set (CBS) limit (see later).[29] Single-point calculations were carried out at RI-MP2/cc-pVQZ//RI-MP2/cc-pVTZ and RI-MP2/cc-pVTZ//RI-MP2/cc-pVDZ levels.

We performed extrapolation to the CBS limit to overcome the slow convergence of the correlation energy, using the extrapolation scheme of Helgaker and co-workers [Eq. (1)],[30] in which E_X and E_{CBS} are energies for the basis set with the largest angular momentum X and for the complete basis set (CBS), respectively. CBS CCSD(T) relative energies were calculated with Equation (2), in which the first term represents the CBS limit of the relative MP2 energy and the second term describes the higher-order contributions to the correlation energy (beyond the second perturbation order).

$$E_X^{HF} = E_{CBS}^{HF} + A\exp(-\alpha X)$$
$$E_X^{corr} = E_{CBS}^{corr} + BX^{-3} \quad (1)$$

$$E_{CBS}^{CCSD(T)} = E_{CBS}^{MP2} + (E^{CCSD(T)} - E^{MP2})|_{small\ basis\ set} \quad (2)$$

This difference is known to not significantly depend on the AO basis set size (contrary to MP2 and CCSD(T) energies).[31] Previous studies[32] have shown that the 6–31G*(0.25) basis set provides a satisfactory value of the CCSD(T)-MP2 difference for molecular clusters, and thus we systematically used this basis set for all present CCSD(T) calculations.

We calculated harmonic vibrational frequencies using a numerical Hessian with a scaling factor of $f = 0.956$. This factor was obtained as the ratio between the theoretical and experimental OH stretch frequencies of FGG. In order to compare theoretical data with experimental enthalpies, we determined the zero-point vibrational energy (ZPVE) from the calculated harmonic vibration frequencies. We determined thermodynamic characteristics (entropy and free energy) from calculated geometries and vibrational frequencies using the rigid rotor/harmonic oscillator/ideal gas approximation (RR-OHO-IG). Thermodynamic characteristics determined in this way are based on the MP2/cc-pVDZ ab initio molecular constants (in contrast to the characteristics derived from MD/Q simulations, which are based on empirical potential description).

Density functional theory calculations: DFT calculations are today widely used for predicting structures and energies of isolated systems as well as of molecular clusters. Introduction of hybrid functionals has increased the accuracy of DFT methods to the point of becoming comparable to the accuracy of correlated ab initio methods. An important advantage of DFT methods over correlated ab initio methods is their favorable CPU performance, which allows the application of DFT techniques to systems of increasing size and complexity. There is, however, one notorious drawback of DFT techniques in their inability to properly describe the London dispersion energy. A most spectacular demonstration of this problem can be seen in the failure of any DFT functional to describe stacking of nucleic acid bases.[33] In our recent paper we have shown that DFT methods also strongly underestimate such interactions in amino acids, and, particularly, that they are unable to describe the rather strong attraction (~10 kcal mol^{-1}) between phenylalanine and a peptide bond.[44] In the present study we used four different functionals, namely BLYP, B3LYP, PBE, and PW91[34–37] as well as two different basis sets, 6–31G(d,p)[38] and cc-pVTZ.[26,27] DFT optimizations were performed at B3LYP/6–31G(d,p) level of theory, while single-point calculations were done at the F/6–31G(d,p)//B3LYP/6–31G(d,p) level (in which F = BLYP, PBE, and PW91) as well as at the B3LYP/cc-pVTZ//B3LYP/6–31G(d,p) level of theory.

Codes: Energies, geometries, harmonic vibrational frequencies, and thermodynamic characteristics were determined using the TURBOMOLE 5.6.[39] DFT optimizations were performed using the Gaussian 03 program package.[40] CCSD(T) calculations were done by using the MOLPRO 2002.6 suite of programs.[41] MD/Q simulations were performed using the AMBER 8.0[42] as well as SCC-DFTB-D[20] codes. CHARMM calculations were done using the Accelrys software package.[18]

Results and Discussion

Spectroscopy: Figure 1 shows the R2PI spectrum of FGG together with UV/UV double-resonance spectra. We found four conformations. Three of these resemble the spectra of Phe and of Phe-Gly, while the origin of the fourth one is significantly red-shifted, by 180 cm^{-1} relative to the other three

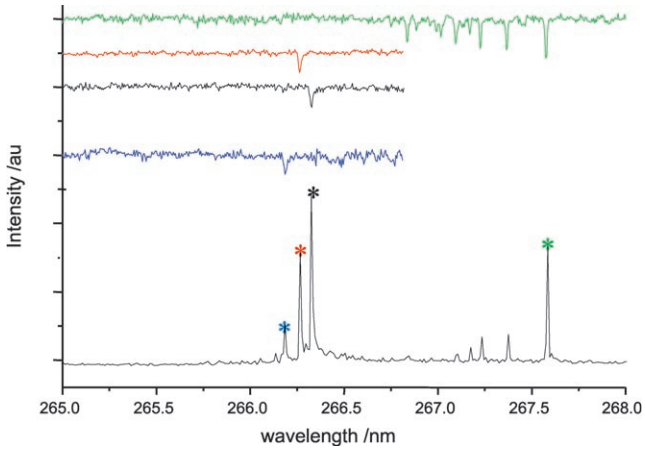

Figure 1. R2PI and UV/UV hole-burning spectra of FGG.

conformations. In earlier work we speculated that this conformation might have a geometric structure distinct from the other three, involving an interaction of the C terminus with the phenyl ring.[43] Figure 2 shows the IR/UV double-resonance spectra, obtained with the probe laser tuned to each of the four origins of the respective conformers. In the following sections we shall compare calculated normal mode frequencies with the experimental IR data.

Strategy of calculations: The case of FGG is complicated, since the system contains several proton donors (NH bonds from two peptide bonds and the OH group), several proton acceptors (oxygen atoms from the C=O bonds of peptide bonds, the nitrogen atom from the amino group, and the oxygen atom from the OH group), and, moreover, regions

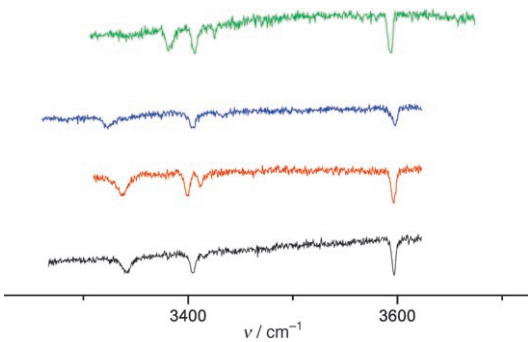

Figure 2. IR/UV hole-burning spectra of FGG, obtained with the probe laser tuned to the respective origins of the four isomer spectra shown in Figure 1.

of delocalized electrons (peptide bonds, aromatic ring, and carboxylic acid) (see Scheme 1). All these areas can interact through the formation of hydrogen bond, electrostatic, or

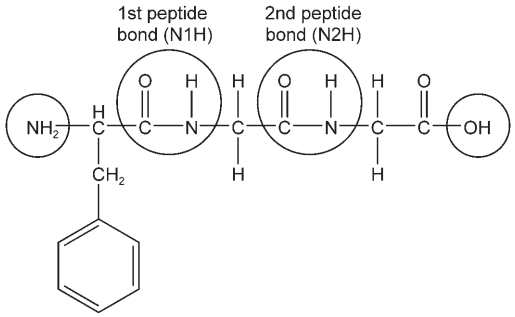

Scheme 1.

dispersion interactions and this complexity leads to a great variety of PESs. The large number of attraction sites also explains why the effectiveness of classical gradient optimization is limited.

The PES of the FGG (as well as of any peptide) is thus very complicated and contains a large number of energy minima separated by transition structures. Evaluation of the deepest minimum structures that can be detected experimentally is thus very difficult and the use of accurate quantum chemical procedures is limited. The PES is usually scanned by using empirical potentials (EP). MD simulations and energy minima are determined by using molecular annealing or quenching procedures. The former procedure aims to determine the global minimum, while the latter one locates all energy minima at the surface. For the present purposes the quenching procedure is more suitable, since the experiment yields several of the deepest energy minima rather than only the global minimum. We note that the present experiments cannot measure relative energies and cannot determine which structure represents a global minimum; this fundamental information can only be obtained theoretically. Very recently it was provided experimentally.[44] By performing MD/Q calculations, one obtains global and local energy minima. However, geometries as well as energies rely on the EP used and different potentials might lead to different sets of energy minima. We suggest several possible approaches to overcome this basic limitation; these are summarized in Scheme 2 and specific routes will be briefly discussed in the following paragraphs.

Route 1: We first explored the PES by a MD/Q[45,46] procedure using the Cornell et al. empirical potential[16] (route 1 in Scheme 2) and we considered approximately 1500 energy minima. As the crystal structure of FGG shows a compact structure, from this set we selected only compact (folded) structures (with the distance between phenyl ring and carboxylic group smaller than 4 Å) and for the 100 lowest-energy folded structures we performed single-point calculations (without any geometry optimization) using correlated ab initio quantum chemical calculations. As a final step we performed a full gradient optimization at higher correlated ab initio level for structures with a relative energy lower than 6 kcal mol^{-1} (set 1).

The above procedure combines the accuracy of the correlated quantum chemical calculations with the efficiency of MD/Q EP calculations. It depends, however, on the ability of the EP used to correctly describe the relative energies of the peptide. If this requirement is not fulfilled then several structures with unfavorable relative empirical energies are excluded from the further, more accurate treatment. Because accurate quantum chemical methods cannot be applied for the first screening (in the present system about 1500 structures should be considered), the only chance to avoid this problem *typical for all biomacromolecules* is to use a higher quality initial screening method. The choice of such a method is limited and there exist only two possibilities.

1) First, improvement can be expected from application of a polarized force field, that is, from inclusion of a polarization (induction) term.[47] The presence of this term avoids one of the main problems of the application of EP for peptides and proteins, namely, the dependence of atomic charges on structural arrangement.[48] As an example we mention the PES of the simplest amino acid, glycine, which contains 12 isomers, for which atomic charges determined by a standard RESP procedure differ considerably.[47] In the present paper we applied two empirical potentials most frequently used for simulations of peptides and proteins (AMBER and CHARMM). Furthermore, we utilized the standard as well as the polarized version of the latter potential.
2) Second, higher-level results can be expected when the first screening of the PES is performed by using some ab initio variational methods that, by definition, overcome the problem of the definition of atomic charges and also the inability of force fields to describe the effect of the electron transfer. Carr–Parrinello ab initio MD simulations[49] represent a possibility, but are impractical for the present purposes. The reason is that the DFT proce-

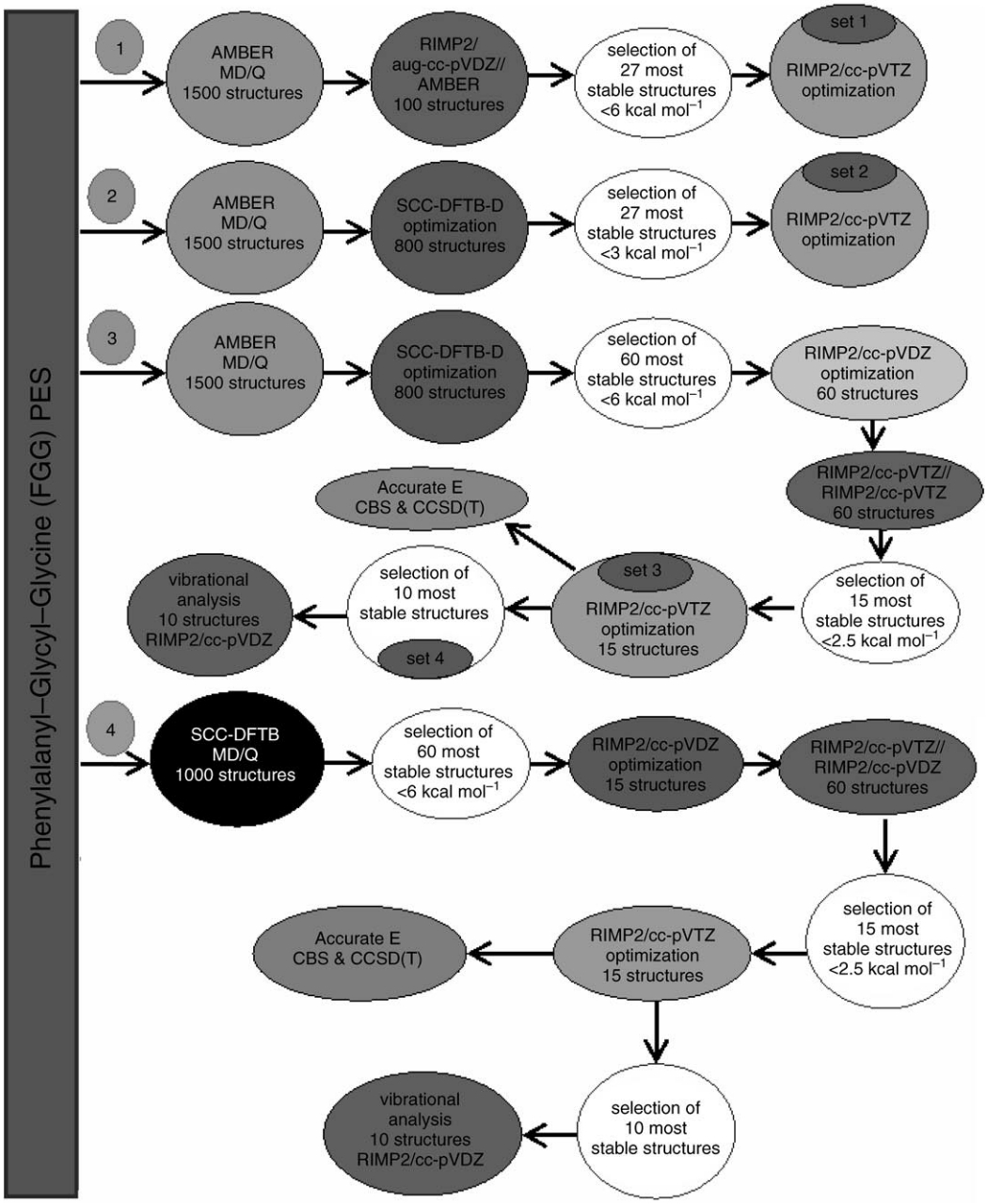

Scheme 2.

dure used (as well as any other DFT procedure) fails to describe the London dispersion energy.[50] Note that the stabilization of FGG tripeptide as well as of other peptides is due to simultaneous action of hydrogen bonding and London dispersion energy. Any method used for description of a conformational space of peptides or proteins should properly describe all major stabilizing forces, including London dispersion. Another possibility is the use of the self-consistent charge, density functional tight-binding method combined with London dispersion energy (SCC-DFTB-D).[20,21] We have recently shown that this method describes the attraction between stacked DNA bases as well as between a phenyl ring and a peptide bond quite successfully, as opposed to various generally used DFT functionals, which fail completely.[44,33,49]

Route 2: In the second step (route 2 in Scheme 2) we investigated the FGG PES by a combination of AMBER, SCC-DFTB-D, and correlated ab initio calculations. Specifically, we first reoptimized the whole set of structures obtained from the initial AMBER MD/Q treatment at the SCC-DFTB-D level. Then, this set of 1500 minima was reduced to 800 structures by a sorting and selection procedure developed for this purpose (see Computational Methods). Finally,

similarly as in route 1, we selected a set of 27 structures (with relative energies lower than 3 kcal mol^{-1}) and compared them with the final set (set 1) resulting from route 1 in Scheme 2. The new set (set 2) was optimized by using a full gradient optimization at correlated ab initio level.

Route 3: The procedure described in route 2 is of higher quality than that described in route 1, but still some problems remain, mainly with the quality of SCC-DFTB-D energies, which directly determines the order of the structures. To improve route 2 we propose in the third step (route 3 in Scheme 2) a combination of several different calculations: 1) The first two calculation steps remained the same as in route 2, 2) structures with a relative energy lower than 4 kcal mol^{-1} from the SCC-DFTB-D calculations were fully reoptimized at a medium ab initio correlated level (RI-MP2/cc-pVDZ), 3) energies of these structures were determined at higher ab initio MP2 correlated level (RI-MP2/cc-pVTZ//RI-MP2/cc-pVDZ; single-point calculations), and 4) structures with relative energy lower than 2.5 kcal mol^{-1} (15 structures) were fully re-optimized at the RI-MP2/cc-pVTZ level of theory. For these 15 selected structures we determined accurate total energies (sum of complete basis set (CBS) limit of the MP2 energy and the CCSD(T) correction term). Finally, we performed a harmonic vibrational analysis for these structures.

Route 4: A fully consistent SCC-DFTB-D MD/Q search is described in route 4 in Scheme 2. Here we performed the first screening of the FGG PES by SCC-DFTB-D MD/Q calculations.[20,21] The following steps, including the correlated ab initio calculations, are identical to those in route 3.

Computational results

Structures and relative energies: Applying route 1 (cf. Scheme 2) we obtained about 1500 structures. Then, we selected only compact (folded) structures. For the 100 most stable compact structures (according to the AMBER scale) we performed RI-MP2/aug-cc-pVDZ single-point calculations. Finally, we selected the 27 lowest-energy folded structures (with relative energy lower than 6 kcal mol^{-1}) for a full ab initio optimization. Figure 3 summarizes these structures as well as the RI-MP2/aug-cc-pVDZ relative energies. The

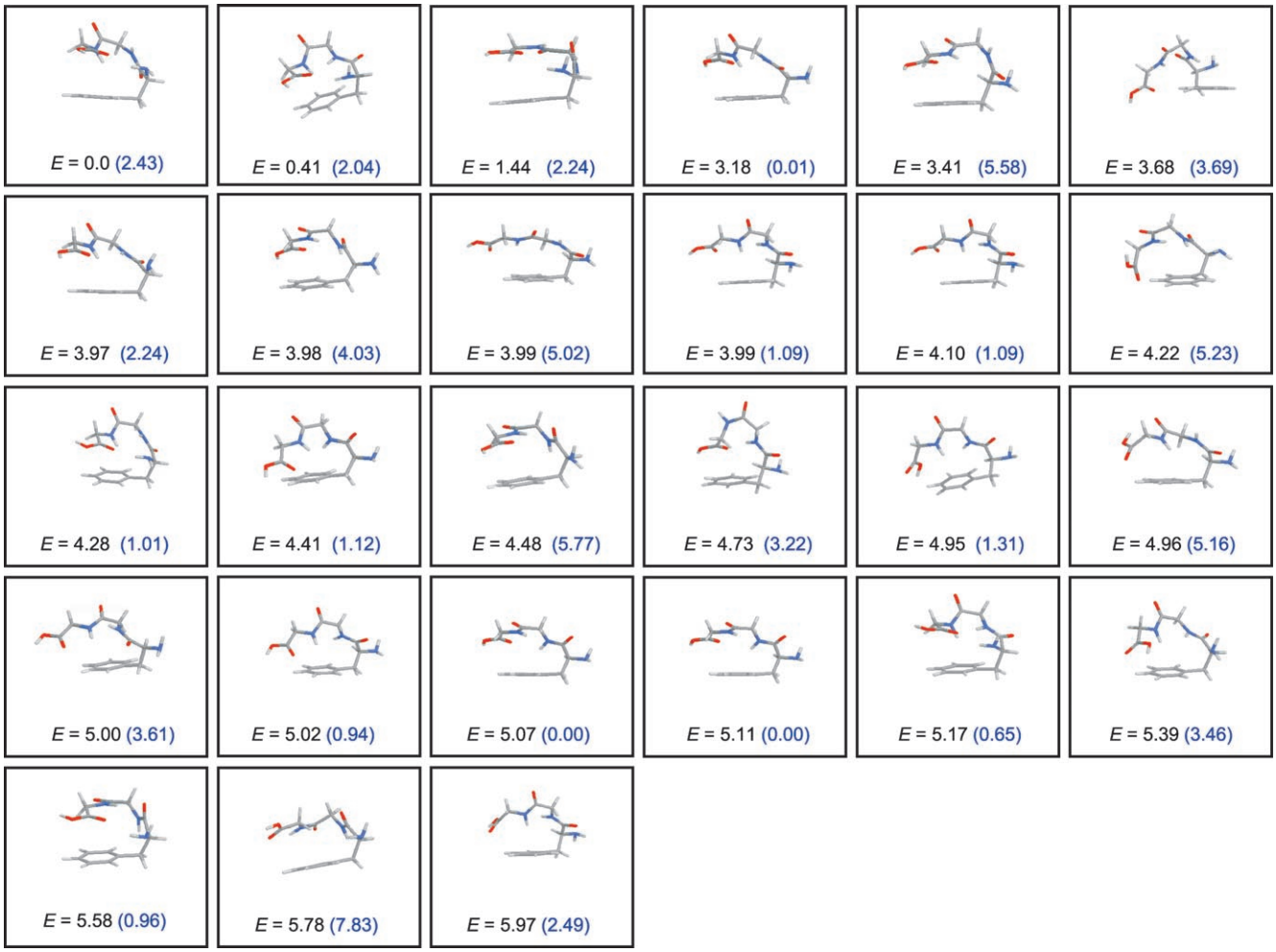

Figure 3. RI-MP2/aug-cc-pVDZ//AMBER and AMBER (in parentheses) geometries and relative energies (in kcal mol^{-1}) for the 27 most stable folded structures according to AMBER scale.

numbers in parentheses are the AMBER relative energies, which differ considerably from the RI-MP2 ones. The RI-MP2 global minimum corresponds to the 14th local minimum at the AMBER scale with a relative energy of 2.4 kcal mol^{-1}. Similarly, the AMBER global minimum corresponds to the 21st local minimum at the RI-MP2 scale with a relative energy of 5.1 kcal mol^{-1}. Evidently, the AMBER potential fails to predict the lowest-energy structures, and their energies are highly unreliable. This observation suggests that AMBER relative energies are of limited use. It also casts some doubts on the selection of lowest-energy structures from Figure 3, since here we used the AMBER geometries. Figure 4 shows results of full RI-MP2/cc-pVTZ optimization (set 1). The number of structures in Figures 3 and 4 differs, since many structures from Figure 3 converged to the same structural motif after optimization. Furthermore, for the sake of comparison, Figure 4 shows the most stable of the fully extended structures (structure in the pink box), although it is higher in energy by about 11 kcal mol^{-1}. Figure 4 shows that the first local minimum is energetically rather close to the global minimum (within about 1 kcal mol^{-1}) and five other structures lie within 5 kcal mol^{-1}. The question now arises of whether the set of initial structures used for the RI-MP2/cc-pVTZ optimization is complete. When analyzing the relative order of the ten most stable structures on the RI-MP2/cc-pVTZ scale we find that they correspond to the 98, 443, 299, 223, 411, 469, 365, 379, 251, and 54th local minima, respectively, on the AMBER scale. Furthermore, from the ten most stable structures on the RI-MP2/cc-pVTZ scale, only two (FGG_54 and FGG_98) appear among the 100 lowest-energy structures on the AMBER scale. From these data it is evident that the initial set of AMBER structures used for the RI-MP2/cc-pVTZ optimizations is far from complete, and consideration of a better initial screening procedure is highly desirable.

To show that the problems described are not specific for the AMBER potential, and to evaluate the performance of the polarized potential, we re-optimized the 27 most stable structures (set 1) from the AMBER optimization using the CHARMM potential (see Table S2 in the Supporting Information). We used the standard version of the code as well as the polarized version, which includes the polarization

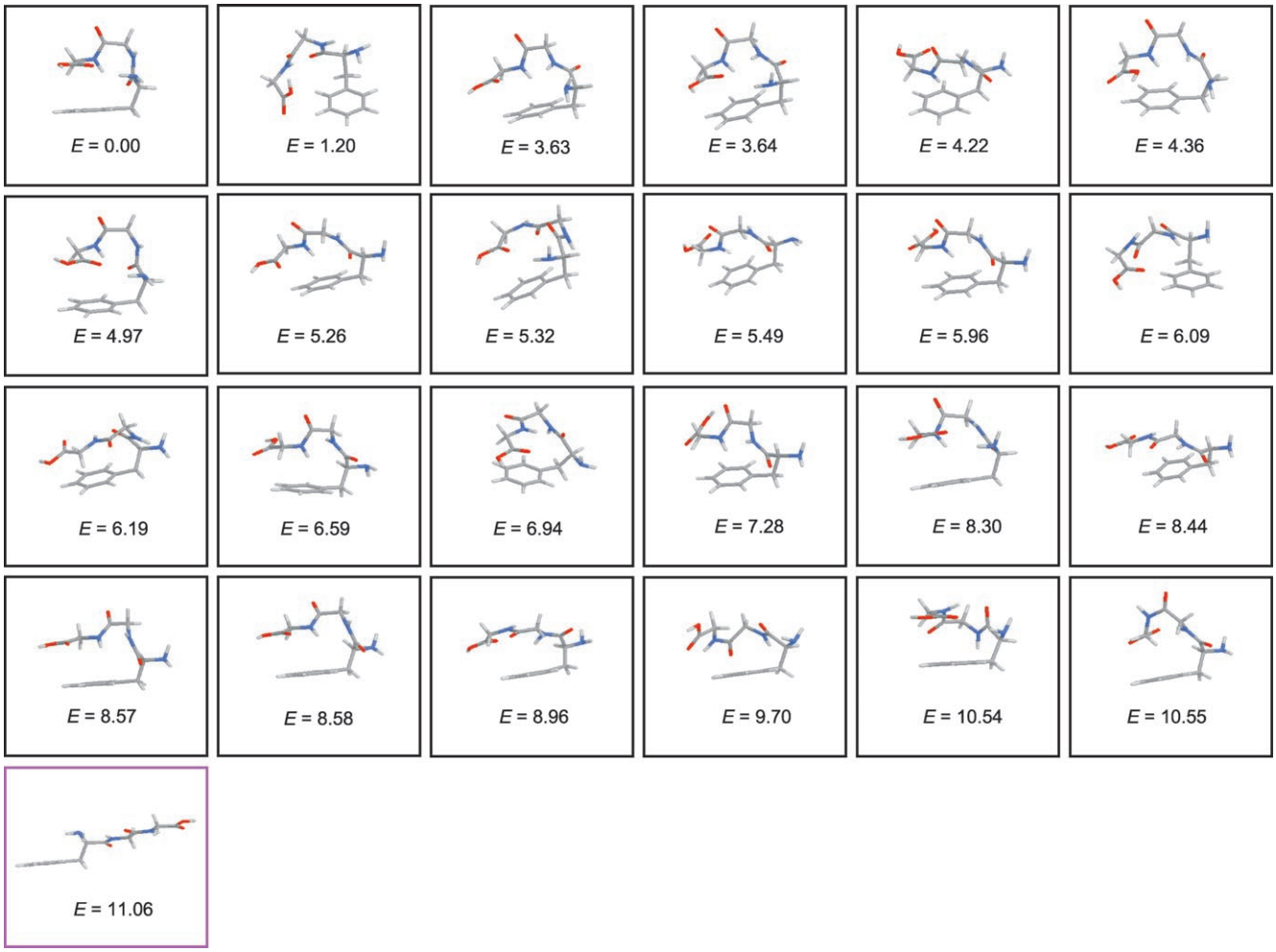

Figure 4. Set 1: RI-MP2/cc-pVTZ geometries and relative energies (in kcal mol^{-1}) for the most stable folded structures at the RI-MP2/aug-cc-pVDZ level of theory.

energy term. In contrast to ab initio and AMBER calculations, CHARMM yielded relative energies in a much narrower interval. Relative energies of the eight energetically most stable structures were located within 1 kcal mol^{-1}. However, the order of stability differed considerably from the ab initio results and the global and the first local minima correspond to the 14th and 17th local minima on the CHARMM scale. The use of the polarized version of CHARMM did not make any significant difference. We can thus conclude that route 1 based on AMBER or CHARMM empirical potentials does not yield satisfactory results.

Route 2 in Scheme 2 differs from route 1 by the introduction of a more reliable fast initial screening procedure (ab initio SCC-DFTB-D method). We applied the method to the entire set of AMBER structures (about 1500 structures). After eliminating repeated minima we obtained a final set of 800 optimized structures. The global minimum and all the structures (27 structures) with relative energy lower than ~3 kcal mol^{-1} (according to the SCC-DFTB-D scale) are depicted in Figure 5 (set 2). The pair of numbers associated with each structure corresponds to the SCC-DFTB-D relative energy and to the RI-MP2/cc-pVTZ relative energy (after optimization in parentheses). Comparing set 2 and set 1 (Figure 4) we find rather little overlap: only four structures, inside the red squares in Figure 5, are present in both sets, underscoring the low fidelity of route 1 based on empirical force fields. For the structures of set 2, the full ab initio gradient optimization at RI-MP2/cc-pVTZ level of theory was performed. From the comparison of RI-MP2/cc-pVTZ and SCC-DFTB-D relative energies it is evident that some problems still remain concerning the order of SCC-DFTB-D energies and this is the reason why the final selection was based on the ab initio treatment described in route 3.

In route 3 (similarly as in route 2) the original set of AMBER structures was reduced via SCC-DFTB-D optimization and subsequently revised and reduced (after elimination of equivalent minima) to a set of about 800 minimum structures. In route 2 we relied on the SCC-DFTB-D relative energies and for ab initio treatment we selected the 27 most stable structures with relative energy of up to ~3 kcal mol^{-1}. Here we adopted a slower (but theoretically more reliable) procedure on a bigger set (about 60 structures with relative SCC-DFTB-D energy lower than ~6 kcal mol^{-1}), and before performing the RI-MP2/cc-pVTZ optimization

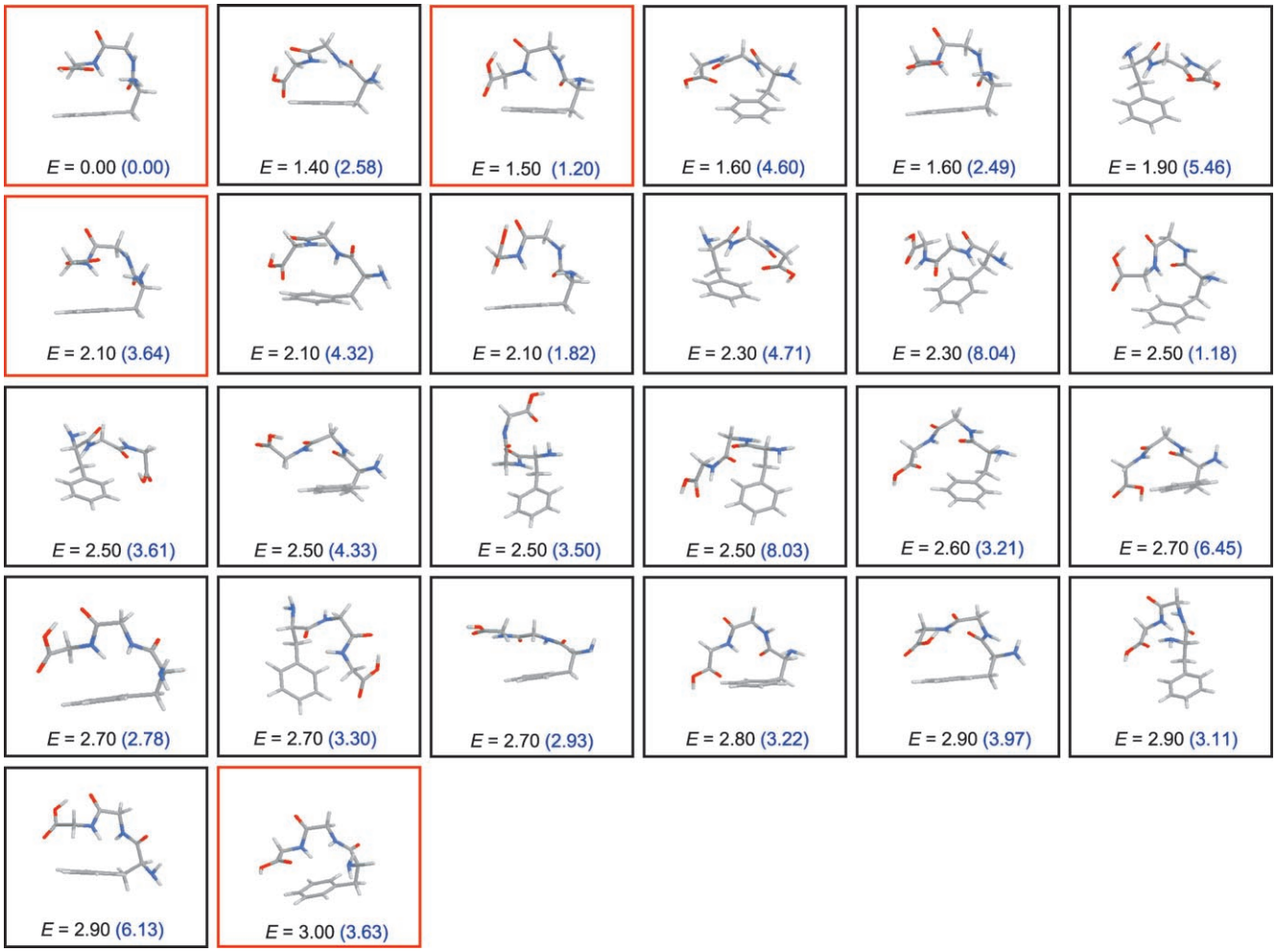

Figure 5. Set 2: SCC-DFTB-D and RI-MP2/cc-pVTZ (in parentheses) geometries and relative energies (in kcal mol^{-1}) for the 27 most stable structures according to SCC-DFTB-D scale.

(which is quite expensive) we applied the much cheaper RI-MP2/cc-pVDZ optimization. We limited this calculation to all SCC-DFTB-D optimized structures lying within a ~6 kcal mol^{-1} energy limit. The selection of the final set of structures for full gradient RI-MP2/cc-pVTZ optimization was performed by means of RI-MP2/cc-pVTZ//RI-MP2/cc-pVDZ single-point calculations. This set (set 3) is depicted in Figure 6 with the structure abbreviation and the RI-MP2/cc-pVTZ relative energies. Table 1 shows the relative RI-MP2/cc-pVTZ and RI-MP2/cc-pVQZ//RI-MP2/cc-pVTZ energies as well as the extrapolated CBS RI-MP2 relative energies. The fifth and sixth column of Table 1 contain the CCSD(T) correction terms and the final relative CBS CCSD(T) energies, respectively, while the last two columns give the zero-point vibration energy (calculated at RI-MP2/cc-pVDZ level of theory) and relative values of total enthalpies. The CCSD(T) correction term ranges from −1.32 to 0.47 kcal mol^{-1}, which means that its omission can cause an error in relative energies of about 2 kcal mol^{-1}. The order of the structures changes when passing from the RI-MP2/cc-pVTZ level of theory (column 2 in Table 1) to the CCSD(T)/CBS level (column 6 in Table 1). The global minimum remains the same, but other structures have different relative positions. The six most stable structures from the former procedure were FGG_099 < FGG_357 < FGG_444 < FGG_215 < FGG_114 < FGG_412 with an energy interval of 2.5 kcal mol^{-1}, while the six most stable structures for the latter procedure were FGG_099 < FGG_444 < FGG_215 < FGG_357 < FGG_366 < FGG_300 with a narrower energy interval of 1.3 kcal mol^{-1}. The CCSD(T)/CBS procedure substantially reduced the relative energies and now the 15 structures presented in Table 1 lie within about 2.5 kcal mol^{-1}. Further reduction of relative energies occurred upon inclusion of ZPE. From the last column of Table 1 it is evident that ten structures lie within 2 kcal mol^{-1} rela-

Table 1. Relative energies and relative enthalpies (in kcal mol^{-1}) of phenyalanyl–glycil–glycine tripeptide evaluated with various basis sets. Numbering as given in Figure 6.

Structure	RI-MP2/ cc-pVTZ	RI-MP2/ cc-pVQZ	T→Q[a]	MP2→CCSD(T)[b]	E[c]	ZPE[d]	H
FGG_099	0.00	0.00	0.00	0.00	0.00	0.00	0.00
FGG_444	1.20	1.05	0.94	−0.80	0.14	0.25	0.39
FGG_357	1.18	0.82	0.57	0.33	0.90	−0.07	0.83
FGG_366	2.95	2.53	2.22	−1.07	1.15	−0.11	0.92
FGG_215	1.82	1.55	1.37	−0.57	0.79	0.14	0.93
FGG_300	3.11	2.83	2.63	−1.32	1.31	−0.15	1.16
FGG_114	1.84	1.58	1.39	0.47	1.87	−0.21	1.66
FGG_412	2.49	2.37	2.29	0.08	2.37	−0.59	1.78
FGG_691	3.52	3.17	2.92	−0.85	2.07	−0.16	1.91
FGG_470	3.21	2.86	2.61	−0.10	2.51	−0.52	1.99
FGG_224	2.58	2.54	2.51	−0.47	2.04	0.06	2.10
FGG_380	3.30	3.01	2.82	−0.51	2.31	–	–
FGG_080	2.78	2.48	2.27	0.26	2.53	–	–
FGG_252	3.50	3.24	3.06	−0.51	2.54	–	–
FGG_055	3.61	3.35	3.17	−0.63	2.54	–	–

[a] Extrapolation to the CBS limit using cc-pVTZ and cc-pVQZ energies. [b] Difference between CCSD(T) and MP2 relative energies determined with the 6–31 g*(0.25) basis set. [c] Total relative energy evaluated as a sum of CBS RI-MP2 relative energy and the difference between CCSD(T) and MP2 relative energies. [d] ZPE were calculated at RIMP2/cc-pVDZ level of theory.

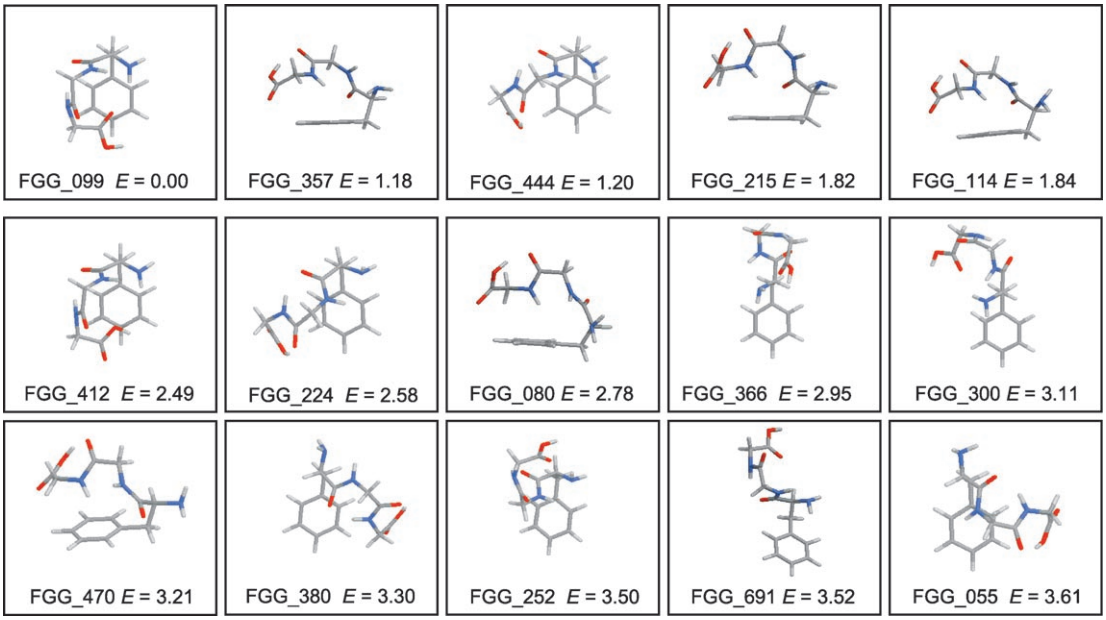

Figure 6. Set 3: RI-MP2/cc-pVTZ geometries and relative energies (in kcal mol^{-1}) for the 15 most stable structures at RI-MP2/cc-pVTZ//RI-MP2/cc-pVDZ level of theory.

tive enthalpy limit and we considered all of them (set 4, Figure 7) for final calculations.

Finally, for the sake of comparison with AMBER MD/Q we performed the first screening of the FGG PES by SCC-DFTB-D MD/Q calculations (route 4 in Scheme 2). The set of structures obtained from this treatment is comparable with the set of structures obtained from the MD(AMBER)/Q(SCC-DFTB-D) one (routes 2 or 3 in Scheme 2). The MD(SCC-DFTB-D)/Q(SCC-DFTB-D) set contains the same structures as the MD(AMBER)/Q(SCC-DFTB-D) one, and, additionally, five new structures appeared (inside the red squares in Figure S2 in the Supporting Information). The SCC-DFTB-D MD/Q procedure is very promising for scanning the PES of tripeptides with important advantages over lower-level MD/Q procedures (see the section on strategy of calculations).

Table 2. Relative energies (in kcal mol^{-1}) of phenyalanyl–glycil–glycine tripeptide evaluated at different levels of theory. Numbering given in Figure 6.

Structure	$E_{CBS}^{CCSD(T)}$ [a]	RI-MP2/ cc-pVDZ	RI-MP2/ cc-pVTZ	B3LYP/ 6–31G(d,p)	SCC-DFTB-D	SCC-DFTB	AMBER	CHARMM
FGG_099	0.00	0.00	0.00	3.56	0.00	0.00	0.89	4.42
FGG_444	0.14	2.13	1.20	0.00	1.47	−1.08	3.69	0.00
FGG_357	0.90	2.45	1.18	–	2.48	0.11	3.13	0.99
FGG_366	1.15	3.60	2.95	1.63	3.84	−0.06	2.05	7.94
FGG_215	0.79	3.00	1.82	0.00	1.47	−1.08	2.35	0.56
FGG_300	1.31	2.98	3.11	1.12	2.90	−0.56	1.28	7.54
FGG_114	1.87	3.27	1.84	1.87	3.36	1.97	1.09	1.54
FGG_412	2.37	4.03	2.49	2.81	1.64	0.54	3.50	4.56
FGG_691	2.07	3.68	3.52	1.91	3.52	−0.07	4.55	9.73
FGG_470	2.51	3.47	3.21	2.45	2.78	1.13	3.67	3.64
FGG_224	2.04	3.74	2.58	0.00	1.42	0.10	2.36	4.16
FGG_380	2.31	4.65	3.30	3.06	2.68	0.52	2.68	1.75
FGG_080	2.53	4.15	2.78	4.87	2.67	1.55	0.61	1.79
FGG_252	2.54	4.11	3.50	3.93	2.53	0.09	1.34	9.19
FGG_055	2.54	4.53	3.61	3.65	2.51	1.05	0.00	2.88

[a] Total relative energy evaluated as a sum of CBS RI-MP2 relative energies and the difference between CCSD(T) and MP2 relative energies.

Final evaluation of the performance of high-, medium-, and low-level methods: We determined the final relative energies of the FGG tripeptide as a sum of CBS RI-MP2 relative energies and a CCSD(T) correction term. Evidently, this very high and expensive level cannot be applied routinely to study the PES of peptides and we would like to evaluate the performance of various lower-level methods. As a trial set we used set 3 (15 structures) presented in Figure 6. Column 2 of Table 2 shows their relative energies determined at the level described above; all these energies lie within 2.5 kcal mol^{-1}. First, we will discuss the performance of RI-MP2/cc-pVDZ and RI-MP2/cc-pVTZ ab initio methods (third and fourth columns of Table 2). A very important point to note is that in both cases the structure of the global minimum remains (FGG_099) and structures FGG_444 and FGG_357 are located close to it. In both cases the relative energy range is larger, but only moderately so (for smaller and larger AO basis set it is 4.7 and 3.6 kcal mol^{-1}, respectively). Working at these levels is evidently safe and any error introduced is not significant.

Next we investigated the performance of the DFT in more detail (for the same trial set—set 3) as is dictated by the importance of the method. Because the structure of the FGG tripeptide is, among other energy contributions, also stabilized by London dispersion energy, the study of the performance of various DFT functionals is topical. The fifth column of Table 2 shows relative energies evaluated at the B3LYP/6–31G** level. The results obtained with three other DFT functionals (BLYP, PBE, and PW91) are not presented, since they are very similar to those obtained with B3LYP, and they are given in Table S3 of the Supporting Information. Analyzing the entries of Table 2 we found that B3LYP results differ strongly from the benchmark data, as well as from both ab initio results. This concerns mainly the position of the global minimum, which is now energetically highly unfavorable (by more than 3.5 kcal mol^{-1}). On the other hand structures that were in the benchmark set local-

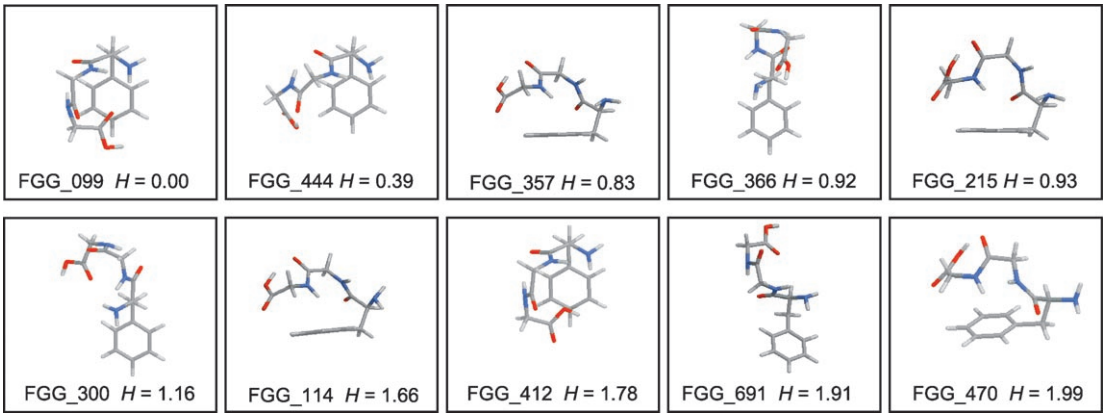

Figure 7. Set 4: Relative enthalpies for the ten most stable structures at the RI-MP2/cc-pVTZ level of theory.

ized energetically above the global minimum now correspond to the global minimum. Evidently the B3LYP functional (and all other DFT functionals investigated) fail to describe the dispersion attraction that critically stabilizes the global minimum (FGG_099). This renders the use of DFT methods questionable for this application.

The sixth column of Table 2 shows relative energies determined by the fast SCC-DFTB-D method. The very strong point of this method is its correct prediction of the global minimum. Relative positions of other structures in the trial set differ from those determined by the most accurate treatment, but the energy interval between the global and 14th local minimum is 3.5 kcal mol^{-1}, which agrees reasonably with the interval (2.5 kcal mol^{-1}) from the most accurate treatment. Reliable relative energies for the SCC-DFTB-D procedure were obtained only because the dispersion energy was covered. The SCC-DFTB method itself fails (cf. the seventh column of Table 2) compared to the standard DFT methods. This once again stresses the importance of dispersion energy in the study of the PES of the FGG tripeptide, and, more generally of all peptides and proteins (see also reference [46]).

Finally, we discuss the performance of empirical force fields. Note that we limit the calculations to structures determined with the RI-MP2/cc-pVTZ optimizations. Column 8 of Table 2 indicates that the AMBER empirical potential fails. The global minimum is predicted to be the structure that in the benchmark set is the 14th local minimum. Furthermore, structures that correspond in the benchmark set to the global and first local minima are now in the trial set as the 2nd and 11th local minima with energy destabilization of 0.9 and 3.7 kcal mol^{-1}. As in the case of AMBER, CHARMM EP (column 9 of Table 2) also fails. The global minimum is now predicted to be the structure that in the benchmark set is the 2nd local minimum, while structures that correspond in the benchmark set to the global and first local minima are now in the trial set the 10th local minimum (with energy destabilization of 4.4 kcal mol^{-1}) and the global minimum, respectively.

Free energy surface (FES) for the final set (set 4 in Figure 7): Because the FGG tripeptide is desorbed at room temperature or higher, the selection of final structures (for which vibration frequencies will be determined and compared with experiment) should be based on the relative free energies, rather than on the relative enthalpies. Table 3 contains the relative populations obtained from the AMBER MD/Q simulations (T=1000 K) as well as the relative free energies and relative populations obtained from the RR-HO-IG (RI-MP2/cc-pVDZ) calculations on the set 4 structures (T= 298 K). These fundamentally different procedures agree on favorable positions of four structures: FGG_099, FGG_366, FGG_300, and FGG_691 (see Figure 8). We expect that only these structures are populated at experimental conditions. The remaining structures (FGG_444, FGG_357, FGG_215, FGG_114, FGG_412, and FGG_470) being energetically very close to the global minimum (by 0.39, 0.83, 0.93, 1.66, 1.78, and 1.99 kcal mol^{-1} (enthalpy values)) are entropically disfavored and will be thus practically not populated. These structures will not be experimentally observed and their calculated IR spectra may be quite different from the experimentally observed spectra.

Table 3. AMBER populations, relative free energies (RI-MP2/cc-pVDZ), and corresponding relative populations calculated according to Maxwell–Boltzmann distribution (MBD) equation for the set 4 (see Figure 7).

Structure	AMBER populations	G [kcal mol^{-1}]	MBD
FGG_099	2205	0.00	1000
FGG_444	37	1.91	41
FGG_357	33	1.90	41
FGG_366	2805	1.61	68
FGG_215	128	2.26	23
FGG_300	6094	0.87	233
FGG_114	290	2.25	23
FGG_412	108	1.65	63
FGG_691	737	1.48	84
FGG_470	165	1.64	64

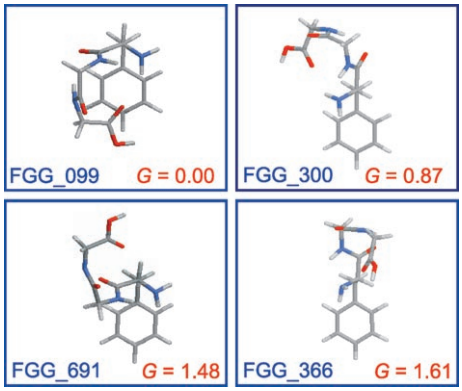

Figure 8. Four most stable structures localized on the free-energy surface.

The global minimum (c.f. Figure 8) contains three hydrogen bonds: (HO)C=O···HN(amino), N(2)H···O=C, and N(1)H···N(amino) having the following O···H and N···H distances: 2.24, 2.05, and 2.12 Å, respectively. On the basis of these distances (all are larger than 2 Å) we can conclude that these hydrogen bonds are not too strong. Surprisingly the global minimum does not contain an expected hydrogen bond between the OH group and the π electrons of the phenyl ring. Evidently, the stacked arrangement of carboxylic group and phenyl ring (containing delocalized π electrons) is energetically more favorable. It is to be noted that our global minimum resembles one of the two structures (structure A) of the Trp–Gly–Gly tripeptide investigated by Hünig and Kleinermanns.[8] The global minimum of the latter peptide is, however, stabilized by two hydrogen bonds, C=O···HN(2) and NH(ind)···O=C(OH), while ours is due to dispersion stabilization between electrons in the carboxylic and phenyl groups. Experimental evidence of this different nature of the interaction can be also found if we have a closer look at the IR spectra of both minima. Whereas for the Trp–Gly–Gly global minimum the free carboxylic acid

ν(OH) and the free indole ν(OH) bands are missing in the spectrum, suggesting their involvement in a hydrogen bond, in the case of the Phe–Gly–Gly the absorption bands for the OH group can be clearly observed. This fact reinforces both the nonexistence of the O–H···π hydrogen bond as well as the important role played by the dispersion interaction in stabilizing the complex.

From Figure 8 it can seen that the global minimum and remaining three minima differ considerably. The "folded" structure is characteristic only for the global minimum, while the other three structures do not contain a close contact between carboxylic and phenyl ring.

Harmonic vibrational analysis for the set of four structures and comparison of theoretical and experimental IR spectra: Hole-burning experiments show the existence of four isomers for which Figure 2 shows the IR spectra. Figure 9 shows the theoretical harmonic (scaled) IR spectra for the ten most stable structures (set 4) together with the most stable of the fully extended structures (cf. structure in the pink box in Figure 4). The IR spectrum of the global minimum (FGG_099) agrees well with the "green" experimental spectrum (cf. Figure 2), and Figure 10 (green curve) shows the overlap of both curves. The OH and N2H stretch frequencies agree to within less than 10 cm^{-1}, while the N1H and asymmetric NH2 stretch frequencies agree to within 20 cm^{-1}. It should be mentioned here that this structure (the global minimum) was not localized if any lower-level theoretical optimization (like DFT) was adopted. It should also be noticed that the FGG_412 structure is geometrically very similar to the global minimum (cf. Figure 9a and h). Actually, the only difference between these two structures is the position of the hydrogen atom of the carboxyl group (in FGG_412 the OH is closer to the amino group, see Scheme 1). We expect that both structures have similar UV spectra and, therefore, the IR spectra of both structures could be measured simultaneously. It may also happen that both spectra are overlapped (see Figure S3 in the Supporting Information). As FGG_412 is less populated than FGG_099 (see Table 3), the spectrum resulting from the weighted overlapping spectra is evidently closer to that of FGG_099.

The scaled harmonic spectra of the first, second, fourth, and sixth local minima (cf. Figure 9b, c, e, g) differ considerably from all the other experimental spectra and the main discrepancy is the very large red-shift of the OH stretch frequency. Inspecting the structures of these four local minima, we find strong hydrogen bonding between the hydrogen atom from the OH group and the oxygen atom from the second peptide bond (see Scheme 1). The common feature of all experimental curves (cf. Figure 2) is a practically identical OH stretch frequency, which indicates no interaction of this group with other proton-acceptor or -donor groups. As discussed above, these local minima are entropically unfavorable and their population at the temperature of the experiment will be negligible.

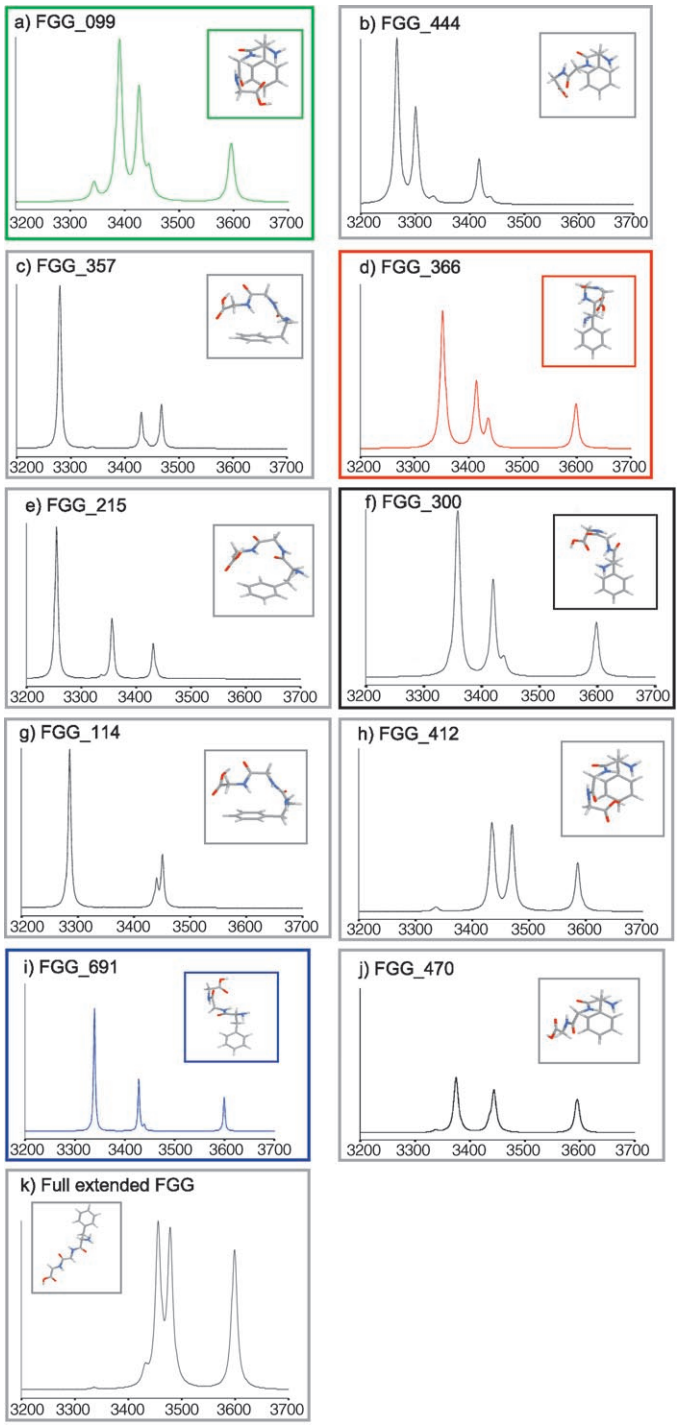

Figure 9. Theoretical harmonic (scaled) IR spectra for the structures of set 4 as well as for the most stable of the fully extended structures.

The IR spectrum of the 3rd local minimum (Figure 9d) agrees well with the IR spectrum of the "red" experimental curve (Figure 2) and the overlap of both curves is depicted in Figure 10 (red curve). The OH stretch frequency agrees within 2 cm^{-1}, while the N1H and N2H stretch frequencies agree to within 17 cm^{-1}, the NH_2 asymmetric stretch frequency differs by 25 cm^{-1}, and, finally, the NH_2 symmetric

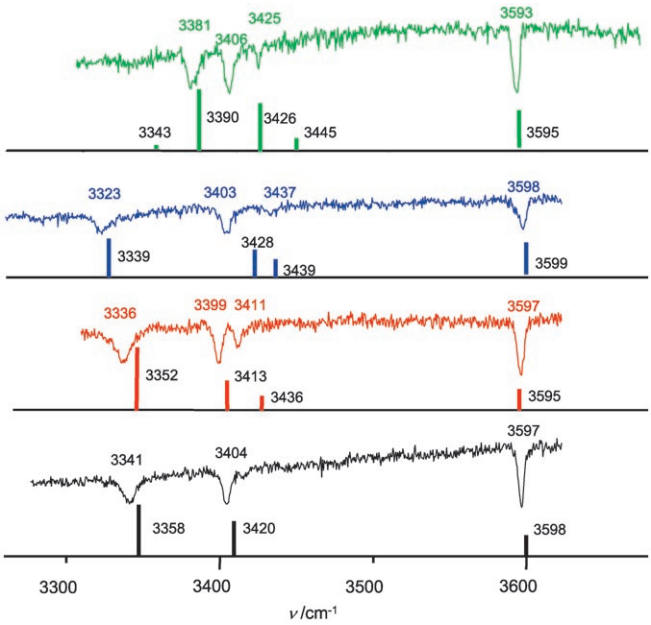

Figure 10. Overlap between theoretical and experimental IR spectra (harmonic vibrational).

stretch frequency is not observed experimentally. The IR spectrum of the 5th local minimum (cf. Figure 9f) agrees well with the IR spectrum of the "black" experimental curve (Figure 2) and the overlap of both curves is depicted in Figure 10 (black curve). The OH stretch frequency agrees within less than 1 cm^{-1}, while the N1H and N2H stretch frequencies differ by less than 17 cm^{-1}. In this case, neither the NH_2 symmetric nor the NH_2 asymmetric frequencies are observed experimentally. Finally, the IR spectrum of the 8th local minimum (Figure 9i) agrees well with the "blue" experimental curve (Figure 2) and the overlap of both curves is depicted in Figure 10 (blue curve). The OH stretch frequency is located within less than 1 cm^{-1}, while N1H stretch frequency differs by 9 cm^{-1}, N2H differs by 16 cm^{-1}, the NH_2 asymmetric stretch frequency differs by approximately 36 cm^{-1}, and NH_2 symmetric stretch frequency is not observed experimentally.

For the sake of comparison we also determined the IR spectrum of the fully extended structure (Figure 9k), which is energetically located more than 11 kcal mol^{-1} above the global minimum (see the structure in the pink box in Figure 4). This structure clearly cannot be detected experimentally and its spectrum differs considerably from experimental ones.

Let us mention finally that the only existing crystal structure of FGG in the Cambridge Structural Database (code FIZWI001)[51] nicely resembles the FGG global minimum in the gas phase. The main discrepancies are due to the different charge distribution in the neutral and zwitterionic form. In contrast to the neutral form, in the crystal structure, no intramolecular hydrogen bonds occur.

Conclusions

1) The hole-burning experiments show that at experimental conditions only four structures of the FGG tripetide coexist, and we recorded their IR/UV double-resonance spectra in the near IR range (3000–4000 cm^{-1}).
2) The PES of the FGG tripeptide contains a large number of energy minima (more than 1000) and an efficient energy-screening strategy is required to exclude higher-energy structures. Stabilization inside the peptide originates in various hydrogen-bonding, electrostatic, and dispersion interactions and their theoretical description is difficult. Frequently used empirical potentials like AMBER or CHARMM fail and the same is true for popular DFT methods. Specifically, these methods are not able to describe the stabilization resulting from the London dispersion energy. The problem was overcome by performing an initial screening with a semi-empirical tight-binding method that covers the London dispersion energy (SCC-DFTB-D). Localization of the lowest-energy structures thus represents a critical key step and currently used procedures are not adequate.
3) Structure and relative energies of the 15 lowest-energy isomers were finally determined on the basis of complete basis set limit RI-MP2 energy and a CCSD(T)/6–31G*-(0.25) correction term (evaluated for the RI-MP2/cc-pVTZ optimized geometries).
4) Since in our beam experiments the conformations are frozen by cooling from a higher temperature, it is necessary to localize the most stable structures on the free-energy surface, rather than on the PES. Two basically different procedures were used to accomplish this and they yield four structures, the global minimum and three local minima. The fact that lowest-energy structures are localized at the FES and not at the PES represents another critical step in the procedure.
5) The global minimum corresponds to a folded structure stabilized, in addition to the two hydrogen bonds, by a dispersion attraction between the phenyl and carboxylic groups. Only the high-level quantum chemical and the SCC-DFTB-D calculations were able to assign this structure as a global minimum. Other lower-level procedures (DFT methods, empirical potentials) localize this structure energetically much higher.
6) We determined scaled vibration frequencies for the ten lowest-energy structures and for four of them a reasonable agreement with experimental data resulted. These four structures were identical with the four lowest-free-energy structures.
7) On the basis of the present paper we suggest a new strategy for the study of peptides. We recommend the use of route 4 in Scheme 2. The only difference from the present procedure is that, instead of using AMBER for the first screening, we will use the SCC-DFTB-D method.

Acknowledgements

This work has been part of the research project Z4 055 905 and was supported by grants from the Grant agency of the Academy of Sciences of the Czech Republic (grant No. A400550510) and Ministry of Education of the Czech Republic (Center for Biomolecules and Complex Molecular Systems, CL512). H.V. holds the EMBO scholarship (Grant ALTF 580–2003) and is supported by the National Science Foundation under contract No. CHE-0244341.

[1] R. J. Petrella, M. Karplus, *J. Mol. Biol.* **2001**, *312*, 1161.
[2] S. G. Pennathur, R. Anishetty, *BMC Struct. Biol.* **2002**, *2*, 9.
[3] G. Duan, V. H. Smith, Jr., D. F. Weaver, *Int. J. Quantum Chem.* **2002**, *90*, 669.
[4] J. Vondrášek, L. Bendová, V. Klusák, P. Hobza, *J. Am. Chem. Soc.* **2005**, *127*, 2615.
[5] L. C. Snoek, E. G. Robertson, R. T. Kroemer, J. P. Simons, *Chem. Phys. Lett.* **2000**, *321*, 49.
[6] L. C. Snoek, R. T. Kroemer, M. R. Hockridge, J. P. Simons, *Phys. Chem. Chem. Phys.* **2001**, *3*, 1819.
[7] B. C. Dian, A. Longarte, S. Mercier, D. A. Evans, D. J. Wales, T. S. Zwier, *J. Chem. Phys.* **2002**, *117*, 10688.
[8] I. Hünig, K. Kleinermanns, *Phys. Chem. Chem. Phys.* **2004**, *6*, 2650.
[9] M. Gerhards, C. Unterberg, A. Gerlach, *Phys. Chem. Chem. Phys.* **2002**, *4*, 5563.
[10] W. Chin, M. Mons, J. P. Dognon, F. Piuzzi, B. Tardivel, I. Dimicoli, *Phys. Chem. Chem. Phys.* **2004**, *6*, 2700.
[11] I. Compagnon, J, Oomens, J. Bakker, G. Meijer, G. Helden, *Phys. Chem. Chem. Phys.* **2005**, *7*, 13.
[12] C. Desfrancois, S. Carles, J. P. Schermann, *Chem. Rev.* **2000**, *100*, 3943.
[13] G. Meijer, M. S. de Vries, H. E. Hunziker, H. R. Wendt, *Appl. Phys. B* **1990**, *51*, 395.
[14] E. Nir, C. Janzen, P. Imhof, K. Kleinermanns, M. S. de Vries, *J. Chem. Phys.* **2001**, *115*, 4604.
[15] M. Schmitt, H. Muller, K. Kleinermanns, *Chem. Phys. Lett.* **1994**, *218*, 246.
[16] W. D. Cornell, P. Cieplak, C. I. Bayly, I. R. Gould, K. M. Merz, Jr., D. M. Ferguson, D. C. Spellmeyer, T. Fox, J. W. Caldwell, P. A. Kollman, *J. Am. Chem. Soc.* **1995**, *117*, 5179.
[17] C. Bayly, P. Cieplak, W. D. Cornell, P. A. Kollman, *J. Phys. Chem.* **1993**, *97*, 10269.
[18] CHARMM: A Program for Macromolecular Energy, Minimization, and Dynamics Calculations: B. R. Brooks, R. E. Bruccoleri, B. D. Olafson, D. J. States, S. Swaminathan, M. Karplus, *J. Comput. Chem.* **1983**, *4*, 187.
[19] "CHARMM: The Energy Function and Its Parameterization with an Overview of the Program": A. D. MacKerell, Jr., B. Brooks, C. L. Brooks, III, L. Nilsson, B. Roux, Y. Won, M. Karplusin, in *The Encyclopedia of Computational Chemistry, Vol. 1* (Eds.: P. von R. Schleyer, N. L. Allinger, T. Clark, J. Gasteiger, P. A. Kollman, H. F. Schaefer III, P. R. Schreiner), Wiley, Chichester, **1998**, pp. 271–277.
[20] M. Elstner, P. Hobza, T. Frauenheim, S. Suhai, E. Kaxiras, *J. Chem. Phys.* **2001**, *114*, 5149.
[21] M. Elstner, T. Frauenheim, E. Kaxiras, G. Seifert, S. Suhai, *Phys. Status Solidi B* **2000**, *217*, 357.
[22] F. Ryjáček, O. Engkwist, J. Vacek, M. Kratochvíl, P. Hobza, *J. Phys. Chem. A* **2001**, *105*, 1197.
[23] M. Feyereisen, G. Fitzgerald, A. Komornicki, *Chem. Phys. Lett.* **1993**, *208*, 359.
[24] O. Vahtras, J. Almlöf, M. Feyereisen, *Chem. Phys. Lett.* **1993**, *213*, 514.
[25] D. E. Bernholdt, R. J. Harrison, *Chem. Phys. Lett.* **1996**, *250*, 470.
[26] T. H. Dunning, Jr., *J. Chem. Phys.* **1989**, *90*, 1007.
[27] R. A. Kendall, T. H. Dunning, Jr., *J. Chem. Phys.* **1992**, *96*, 6796.
[28] P. Jurečka, P. Nachtigall, P. Hobza, *Phys. Chem. Chem. Phys.* **2001**, *3*, 4578.
[29] T. H. Dunning, Jr., *J. Phys. Chem. A* **2000**, *104*, 9062.
[30] A. Halkier, T. Helgaker, P. Jørgensen, W. Klopper, H. Kock, L. Olsen, A. K. Wilson, *Chem. Phys. Lett.* **1998**, *286*, 243.
[31] P. Jurečka, P. Hobza, *Chem. Phys. Lett.* **2002**, *365*, 89.
[32] P. Hobza, J. Šponer, *J. Am. Chem. Soc.* **2002**, *124*, 11802.
[33] I. Dąbkowska, H. Valdés González, P. Jurečka, P. Hobza, *J. Phys. Chem. A* **2005**, *109*, 1131.
[34] C. Lee, W. Yang, R. G. Parr, *Phys. Rev. B* **1988**, *37*, 785.
[35] A. D. Becke, *Phys. Rev. A* **1988** *38*, 3098.
[36] K. Burke, J. P. Perdew, Y. Wang, *Electronic Density Functional Theory: Recent Progress and New Directions* (Eds.: J. F. Dobson, G. Vignale, M. P. Das), Plenum, New York, **1998**.
[37] J. P. Perdew, K. Burke, M. Ernzerhof, *Phys. Rev. Lett.* **1996**, *77*, 3865.
[38] W. J. Hehre, L. Radom, P. von R. Schleyer, J. A. Pople, *Ab initio Molecular Orbital Theory*, Wiley, New York, **1986**.
[39] R. Ahlrichs, M. Bär, M. Häser, H. Horn, C. Kölmel, *Chem. Phys. Lett.* **1989**, *162*, 165.
[40] Gaussian 03, Revision A.1, M. J. Frisch, G. W. Trucks, H. B. Schlegel, G. E. Scuseria, M. A. Robb, J. R. Cheeseman, J. A. Montgomery, Jr., T. Vreven, K. N. Kudin, J. C. Burant, J. M. Millam, S. S. Iyengar, J. Tomasi, V. Barone, B. Mennucci, M. Cossi, G. Scalmani, N. Rega, G. A. Petersson, H. Nakatsuji, M. Hada, M. Ehara, K. Toyota, R. Fukuda, J. Hasegawa, M. Ishida, T. Nakajima, Y. Honda, O. Kitao, H. Nakai, M. Klene, X. Li, J. E. Knox, H. P. Hratchian, J. B. Cross, V. Bakken, C. Adamo, J. Jaramillo, R. Gomperts, R. E. Stratmann, O. Yazyev, A. J. Austin, R. Cammi, C. Pomelli, J. W. Ochterski, P. Y. Ayala, K. Morokuma, G. A. Voth, P. Salvador, J. J. Dannenberg, V. G. Zakrzewski, S. Dapprich, A. D. Daniels, M. C. Strain, O. Farkas, D. K. Malick, A. D. Rabuck, K. Raghavachari, J. B. Foresman, J. V. Ortiz, Q. Cui, A. G. Baboul, S. Clifford, J. Cioslowski, B. B. Stefanov, G. Liu, A. Liashenko, P. Piskorz, I. Komaromi, R. L. Martin, D. J. Fox, T. Keith, M. A. Al-Laham, C. Y. Peng, A. Nanayakkara, M. Challacombe, P. M. W. Gill, B. Johnson, W. Chen, M. W. Wong, C. Gonzalez, and J. A. Pople, Gaussian, Inc., Wallingford CT, **2003**.
[41] MOLPRO, a package of ab initio programs designed by H.-J. Werner and P. J. Knowles, version 2002.1, R. D. Amos, A. Bernhardsson, A. Berning, P. Celani, D. L. Cooper, M. J. O. Deegan, A. J. Dobbyn, F. Eckert, C. Hampel, G. Hetzer, P. J. Knowles, T. Korona, R. Lindh, A. W. Lloyd, S. J. McNicholas, F. R. Manby, W. Meyer, M. E. Mura, A. Nicklass, P. Palmieri, R. Pitzer, G. Rauhut, M. Schütz, U. Schumann, H. Stoll, A. J. Stone, R. Tarroni, T. Thorsteinsson, H.-J. Werner.
[42] AMBER 6: D. A. Case, T. A. Darden, T. E. Cheatham, III, C. L. Simmerling, J. Wand, R. E. Duke, T. Luo, K. M. Merz, B. Wang, D. A. Pearlman, M. Crowley, S. Brozell, V. Tsui, H. Gohlke, J. Mongan, V. Hornak, G. Cui, P. Beroza, C. Schafmeister, J. W. Caldwell, W. S. Ross, and P. A. Kollman, **2004**, University of California, San Francisco.
[43] R. Cohen, B. Brauer, E. Nir, M. S. De Vries, *J. Phys. Chem. A* **2000**, *104*, 6351.
[44] B. C. Dian, J. R. Clarkson, T. S. Zwier, *Science* **2004**, *303*, 1169.
[45] F. G. Amar, R. S. Berry, *J. Chem. Phys.* **1986**, *85*, 5943; M. F. Stillinger, T. A. Weber, *Phys. Rev. A* **1982**, *23*, 987.
[46] M. Kratochvil, O. Enkvist, J. Šponer, P. Jungwirth, P. Hobza, *J. Phys. Chem. A* **1998**, *102*, 6921.
[47] K. J. Jalkanen, M. Elstner, S, Suhai, *J. Mol. Struct. THEOCHEM* **2004**, *675*, 61.
[48] J. Chocholoušová, J. Vacek, F. Huisken, O. Werhahn, P. Hobza, *J. Phys. Chem. A* **2002**, *106*, 11540.
[49] R. Car, M. Parrinello, *Phys. Rev. Lett.* **1985**, *55*, 2471.
[50] P. Hobza, J. Šponer, *Chem. Rev.* **1999**, *99*, 3247.
[51] E. Subramanian, J. J. Sahayamary, *Int. J. Pept. Protein Res.* **1989**, *34*, 211.

Received: April 25, 2005
Published online: August 10, 2005

